Fuel Matrix Degradation Model: Canister Corrosion and the Effect of Hydrogen on Used Fuel Degradation Rates

Used Fuel Disposition

Prepared for
U.S. Department of Energy
Used Fuel Disposition Campaign
James Jerden
Jacqueline M. Copple
Terry Cruse
William Ebert
Argonne National Laboratory

July 21, 2016
FCRD-UFD-2016-000613 &
FCRD-UFD-2016-000614

This work was supported by the US Department of Energy, Office of Nuclear Energy. The report was prepared at Argonne National Laboratory as part of the Used Fuel Disposition (UFD) Campaign.

SUMMARY

This work is being performed as part of the DOE NE Used Fuel Disposition (UFD) Campaign Argillite and Crystalline Rock R&D work packages: FT-16AN08030201 and FT-16AN08030301. This document meets the July 21, 2016 milestone ANL M4FT-16AN080302011 for Argillite R&D and the July 21, 2016 milestone ANL M4FT-16AN080303011 for Crystalline R&D.

The most important observation is that, due to the effect of H_2 on the fuel degradation rate, the peak dose from released radionuclides will likely be significantly attenuated due to the corrosion of waste package steel components. This indicates that having an accurate model for steel corrosion and the associated H_2 effect is essential for accurate source term calculations within the performance assessment model.

The main purpose of this project is to develop a process model to calculate the degradation rate of used fuel based on fundamental underlying processes that provides radionuclide source terms for the Generic Disposal System Analysis PA model. The primary accomplishments for FY2016 work on the Fuel Matrix Degradation Model (FMDM) development project at Argonne are as follows:

- Formulated, coded and tested an electrochemical steel corrosion module that couples kinetics for in-package steel corrosion with fuel degradation. This module provides the source of H_2 that dominates used fuel dissolution rates under repository relevant conditions.
- Updated and optimized the FMDM to improve the efficiency of integration with the GDSA PA model.
- Performed scoping electrochemical tests to build confidence in modeling the dominant H_2 effect mechanism, which has been shown to significantly impact source term calculations when in-package steel components are corroding simultaneously with used fuel.

The key observation made during the FY-2016 work was that the corrosion of steel canister materials will have significant impact on the radionuclide source terms calculated by PA due to the dominating effect of H_2 at the fuel – solution and NMP – solution interfaces. Calculations made with the updated FMDM indicate that the peak radionuclide source term from a breached waste package will likely be delayed until all of the internal steel components are consumed by corrosion.

These processes are now accounted for in the FMDM V.3; however, there remains a need for coupled experimental and process modeling work to accurately parameterize and validate the model. This future work is particularly important because the FMDM is currently being used to provide the radionuclide source term in the PA model. Thus, future improvements to the FMDM process model will have a direct impact on the accuracy of the existing GDSA PA model.

The highest priority FY-2017 activities identified are as follows:

- Extend the FMDM Fortran – PFLOTRAN interface files to account for the corrosion of the steel components and the associated H_2 effect that anodically protects the fuel from oxidative degradation.

- Take next step in integration of FMDM with PA: demonstrate sensitivity of the Argillite PA model to key variables in the FMDM such as burnup, surface area, steel corrosion/H_2 production rates and the dissolved concentrations of H_2, O_2, carbonate and ferrous iron.
- Perform focused electrochemical experiments to determine the effect of halides and other possible poisons on the catalytic efficiency of the NMP. These tests will quantify processes that may counteract the protective H_2 effect.
- Incorporate the effect of poisons (e.g., Br, S) or other processes that counteract the protective H_2 effect into the FMDM.

Furthermore, the recognition and quantification of the interactions between the corrosion of steel waste package components and waste form degradation suggests that models developed for the FMDM may provide important insights as to the types and amounts of steels that could be used to optimize the long-term performance of the waste package and canister materials.

CONTENTS

ACRONYMS

DOE	U.S. Department of Energy
FEPs	features, events, and processes
ICPMS	Inductively coupled plasma mass spectrometry
OCP	Open circuit potential
ORNL	Oak Ridge National Laboratory
PA	performance assessment
R&D	Research and development
SNF	spent nuclear fuel
SEM	scanning electron microscopy
SHE	standard hydrogen electrode
UFD	Used Fuel Disposition Campaign
UNF	used nuclear fuel
MCNPX	Monte Carlo N-Particle eXtended

1. INTRODUCTION AND OBJECTIVE

Scientifically-based predictive models of waste form corrosion rates will provide reliable radionuclide source terms for use in repository performance assessments. Furthermore, demonstrating that there is a fundamentals-based, scientific basis for the waste form degradation process models is a key aspect for building confidence in the long-term calculations used for the repository safety case.

The objective of this project is to develop and implement a fundamentals-based process model for the degradation rate of used fuel that can be readily incorporated into the Generic Disposal System Analyses (GDSA) Performance Assessment (PA) code to provide radionuclide source terms throughout the service life of a disposal system. This model, referred to as the Fuel Matrix Degradation Model (FMDM), is based on the Canadian Mixed Potential Model (King and Kolar, 2003), but has been expanded and customized for application in the ongoing UFD Argillite and Crystalline rock disposal projects. The conceptual context for the FMDM within the generic performance assessment model is shown in Figure 1.

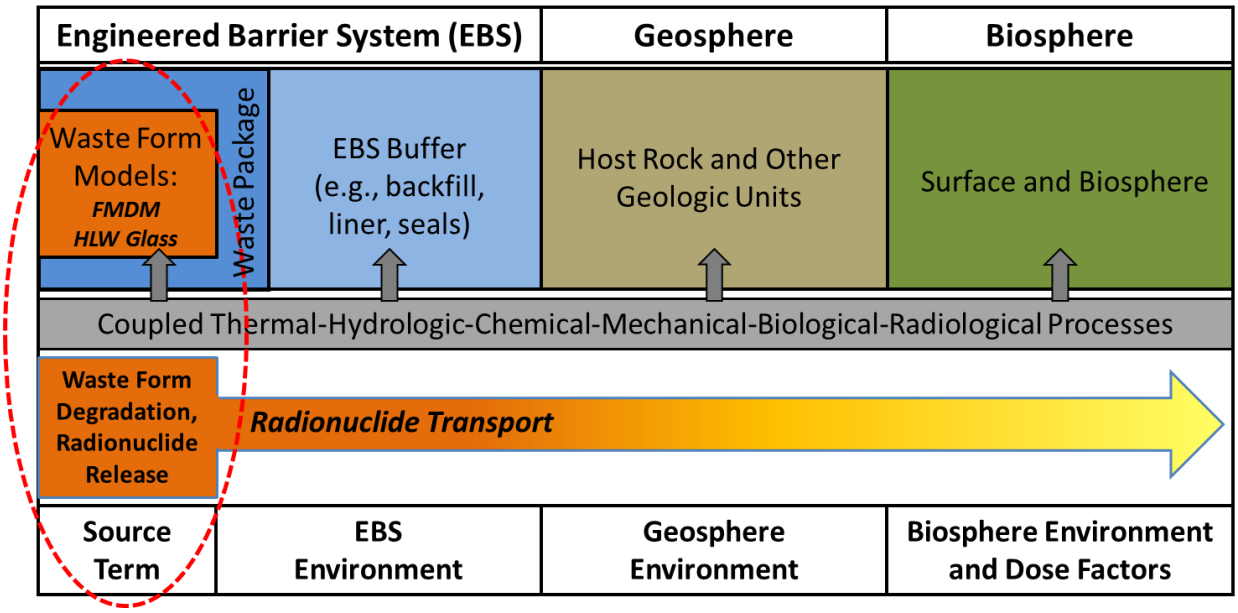

Figure 1. Conceptual diagram showing the context for the FMDM. Adapted from Mariner et al., 2015.

The continued development and implementation of the FMDM addresses two high level Features, Events, and Processes (FEPs) that are recognized as high R&D priorities for the UFD (Wang et al., 2014). The FEPs addressed by this model are 2.1.02 (waste form) and 2.1.03 (waste container), which correspond to the high priority research topics P19 (Development of waste form degradation model) and P20 (Development of new waste package concepts and models for evaluation of waste package performance for long-term disposal) identified by Wang et al., 2014.

The FMDM calculates the dissolution rate of used fuel as a function of the interfacial corrosion potential (E_{corr}) that is determined by the kinetic balance between all of the anodic and cathodic half reactions occurring at the fuel/solution boundary. The dissolution rate is relatively high under oxidizing conditions (high E_{corr}) but decreases dramatically at E_{corr} values lower than the U(IV)/U(VI) threshold potential, where only solubility-based chemical dissolution occurs. The FMDM accounts for:

- the generation of radiolytic oxidants as a function of fuel burn-up,
- the catalyzed oxidation of H_2, which protects the fuel from oxidative dissolution,
- the precipitation of secondary phases,
- the complexation of uranyl by carbonate,
- the oxidation of ferrous iron,
- temperature variations (by Arrhenius equations),
- the one-dimensional diffusion of all chemical species,
- the anoxic corrosion of steel components within a breached waste package to provide the flux of H_2 and ferrous iron, which, as discussed below, dominate fuel degradation process (*added and tested in FY-2016*).

Of these processes, the catalysis of H_2 oxidation on Nobel Metal Particles (NMP) on the fuel surface and the generation rate of radiolytic oxidants (determined by dose rate, which is related to fuel burn-up) are the most important for determining the degradation rate of the fuel (Jerden et al., 2015). Since the flux of H_2 to the fuel is determined by the anoxic corrosion rate of steel waste package components (e.g., Shoesmith, 2008), steel corrosion kinetics were added to the FMDM in FY-2016. The new electrochemical steel corrosion module is discussed in Section 2.

Specifically, the fuel degradation rate calculated by the FMDM accounts for oxidation of the fuel by radiolytic H_2O_2 (and its decomposition product O_2), the concentration of which is calculated using an analytical form of the radiolysis model developed at PNNL (Buck et al., 2014), and the burn-up/dose rate function described in Section 4 of this report. Fuel oxidation is counteracted by the catalytic oxidation of H_2 on NMP sites that are present on the fuel surface as a distinct phase.

It was shown in Jerden et al., 2015 that the FMDM accurately reproduces the experimental observation that relatively low concentrations of dissolved H_2 (~0.1mM) can inhibit the oxidative dissolution of the fuel. In the absence of oxidative dissolution, the fuel degrades by solubility based, chemical dissolution, which is over 4 orders of magnitude slower than oxidative dissolution (Röllin et al., 2001).

The present study, which focuses on the degradation behavior of uranium oxide used fuel, shows that interactions between the seepage water contacting the fuel and engineered barrier materials

should be accounted for in waste form degradation models. As discussed in this report, it is particularly important to account for chemical interactions between the corroding used fuel and steel waste package components that occur through a common solution.

Figure 2 is a conceptual diagram showing the key interfacial and bulk solution reactions included in the new version of the FMDM (FMDM Version 3) as well as other important source term processes that are not yet included, but may play a key role in radionuclide release and transport *(shown in dark red on Figure 2).*

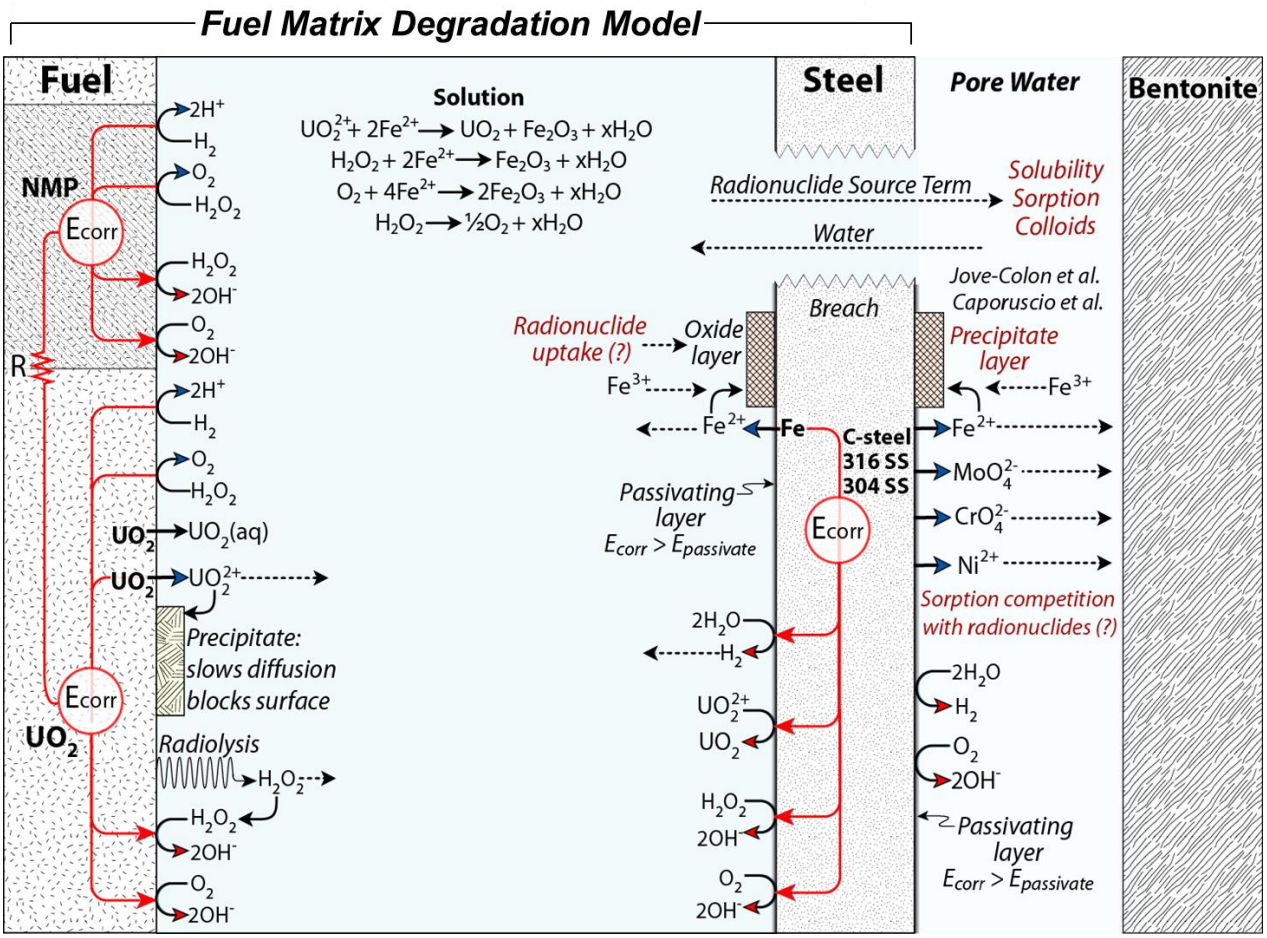

Figure 2. Conceptual diagram showing the context for the FMDM. Adapted from Mariner, P., Gardner, P., Hammond, G, Sevougian, D, Stein E., 2015, Application of Generic Disposal System Models, FCRD-UFD-2015-000126, SAND2015-10037, September 22, 2015, 209pp.

2. FY-2016 EXTENTION OF THE FUEL MATRIX DEGREDATION MODEL: ELECTROCHEMICAL STEEL CORROSION MODULE

Quantification of the long-term corrosion behavior of steels in relevant environmental conditions is central to developing a scientifically sound performance assessment model for nuclear waste repositories. As shown in Figure 3, the used fuel assemblies will be surrounded by and in close contact with steel components within the waste package and disposal canister.

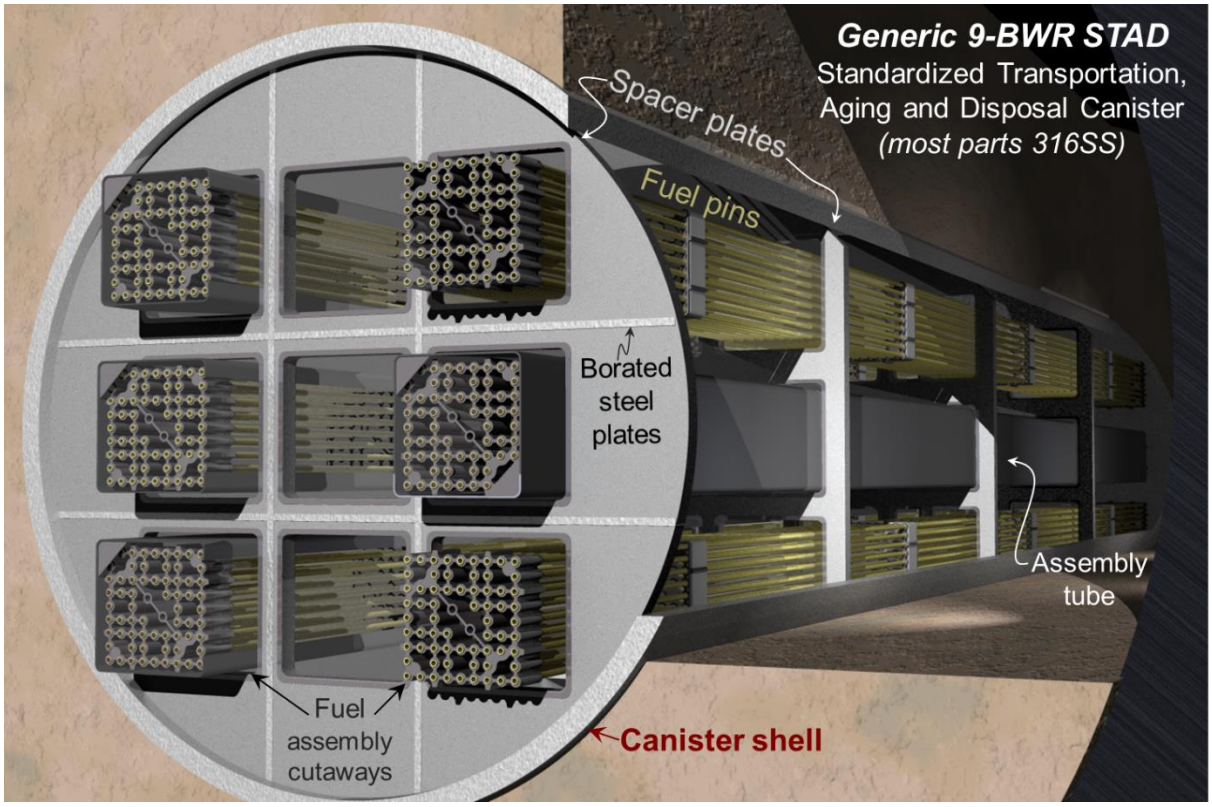

Figure 3. Conceptual diagram showing a generic BWR waste package.

Within a breached canister groundwater will infiltrate open spaces within the canister and begin to corrode steel components (Figure 4). This will set up a reaction front that will eventually contact the fuel rods. The steel will corrode and produce H_2 even if the infiltrating groundwaters are reducing. This is because the stability field of carbon steels and stainless steels lie below the stability field of water on an Eh vs. pH diagram (Figure 5). Therefore, as shown in both Figure 5a and Figure 6 (steel surface), metallic iron can be oxidized to Fe^{2+} by the reduction of water to H_2 + $2OH^-$. Assuming that the Zircaloy cladding has failed, the fuel will begin degrading by either relatively rapid oxidative dissolution or by relatively slow chemical dissolution. The dominant dissolution mechanism will be determined by the surface potential established by the solution contacting the fuel surface.

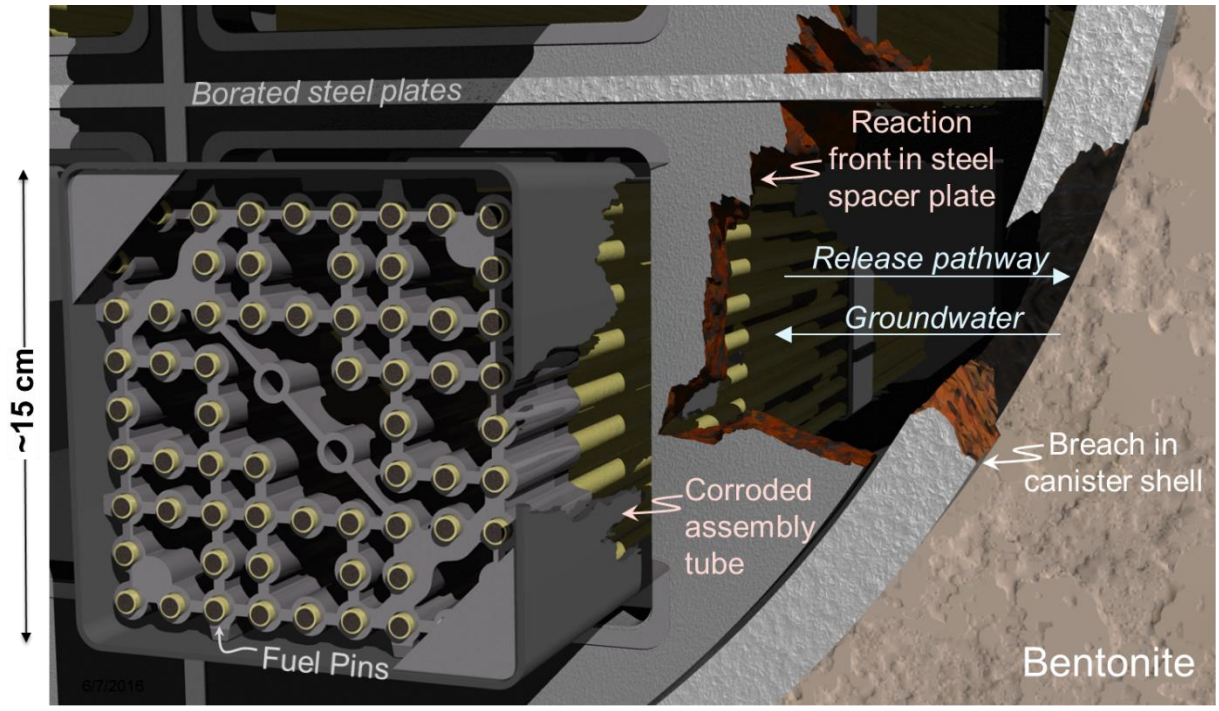

Figure 4. Conceptual diagram summarizing the key processes involved in radionucide release from a breached used fuel waste package. Following a breach groundwater will oxidize steel components and eventually reach fuel rods. The key thing to note is that the used fuel will degrade simultaneously with a number of different types of steels. The interactions between the steel corrosion reaction products H_2 and Fe^{2+} have been shown experimentally strongly effect the rate of fuel degradation (e.g., Shoesmith, 2008, Grambow, et al., 2010).

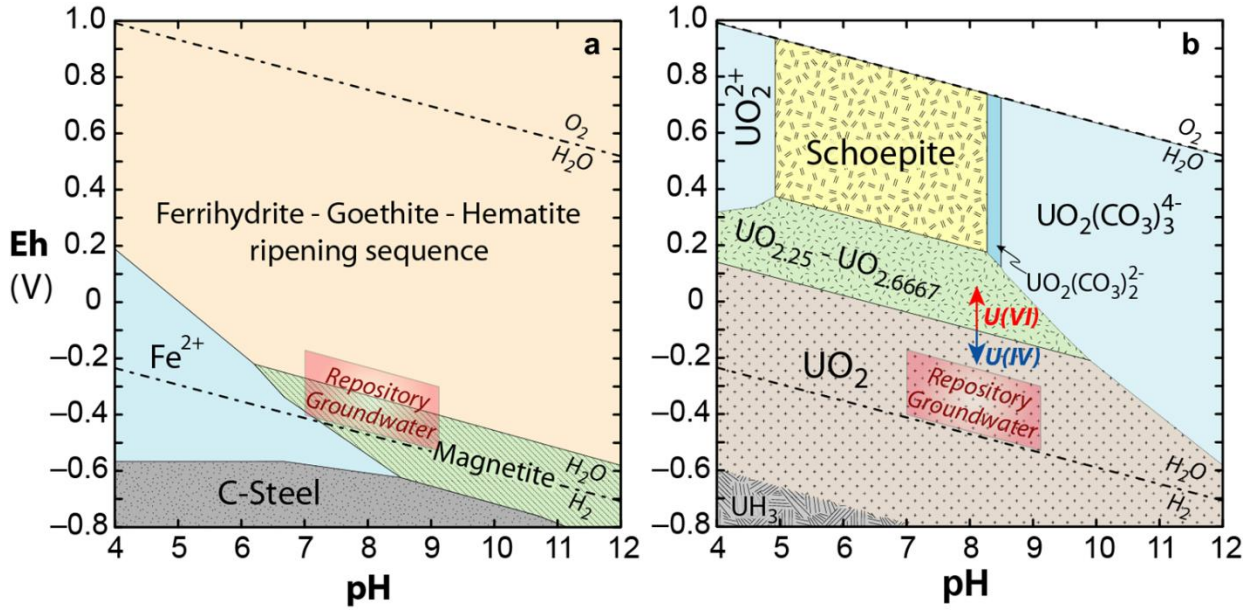

Figure 5. Eh – pH diagrams showing the conditions expected for groundwaters in a reducing crystalline rock or argillite repository (from Laaksoharju, et al., 2008). Figure 5a was drawn for $1x10^{-3}$ molar iron and the 5b was drawn for $1x10^{-6}$ molar uranium with $1x10^{-4}$ molar carbonate.

The rate of fuel degradation will ultimately be determined by the kinetic balance of five processes:

- The rate of radiolytic oxidant production (determined by dose rate, which is determined by fuel burn up and age)
- The rate of radiolytic oxidant reduction on fuel surface (cathodic reactions on fuel surface)
- The rate of U(IV) → U(VI) oxidation (anodic reactions on fuel surface)
- Rate of H_2 production by steel corrosion and H_2 flux to the NMP sites on the fuel surface
- The rate of the oxidation of H_2 on the NMP catalytic sites (anodic reaction on fuel surface that anodically "protect" UO_2 from oxidation)

These processes are shown conceptually in Figure 6, which summarizes the reaction scheme for the FMDM.

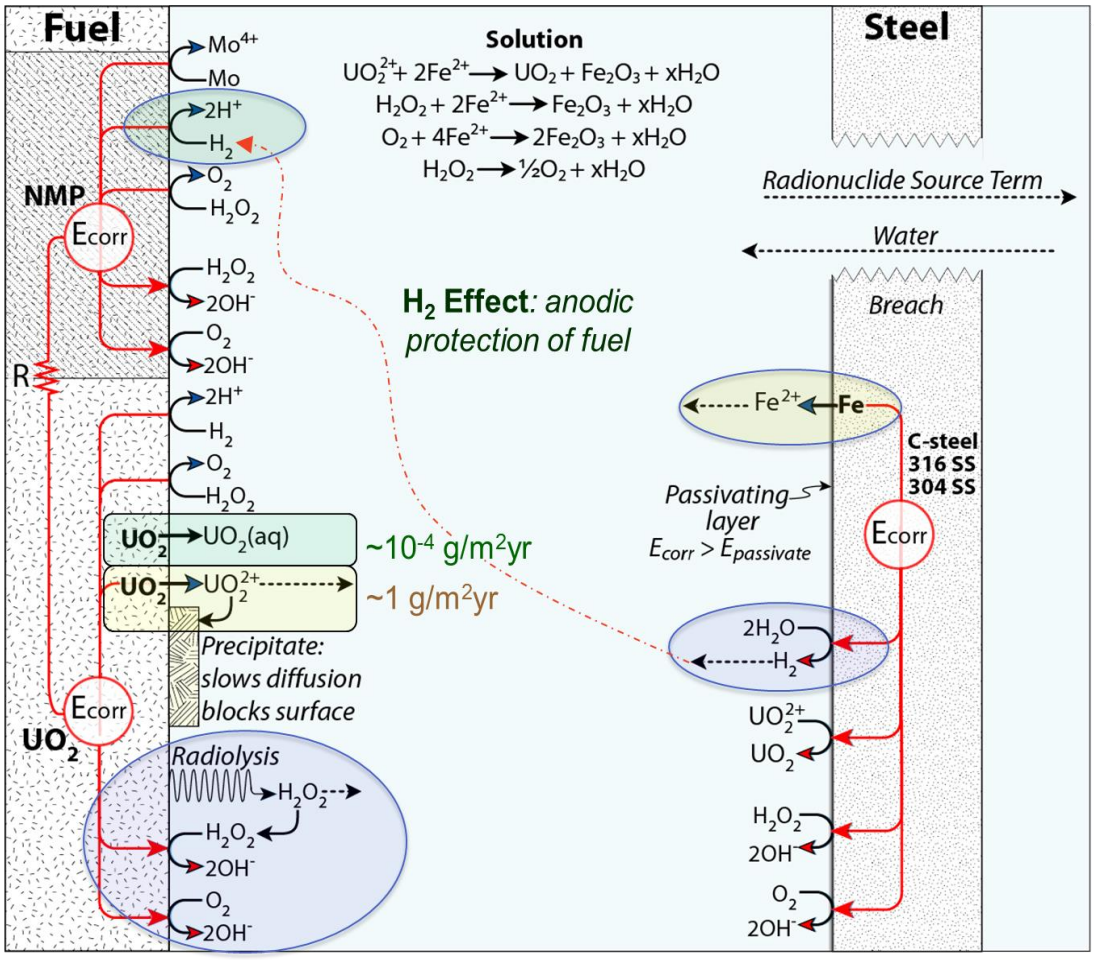

Figure 6. Schematic diagram showing the reaction scheme for the FMDM. The key processes in the model are highlighted in yellow (key anodic reactions), blue (key cathodic reactions) and green (the H_2 effect that can provide anodic protection of the UO_2 matrix from oxidative dissolution).

The mixed potential theory on which the FMDM is based Model (King and Kolar, 2003) is also ideal for quantifying steel corrosion because it accounts for the fundamental interfacial electrochemical reactions and couples those reactions with bulk solution chemistry. Therefore, as part of our FY-2016 work, we formulated, coded, and tested a relatively simple mixed potential model for steel corrosion and then added that model to the FMDM as a new module. The interfaces between the modules is presented in Figure 7.

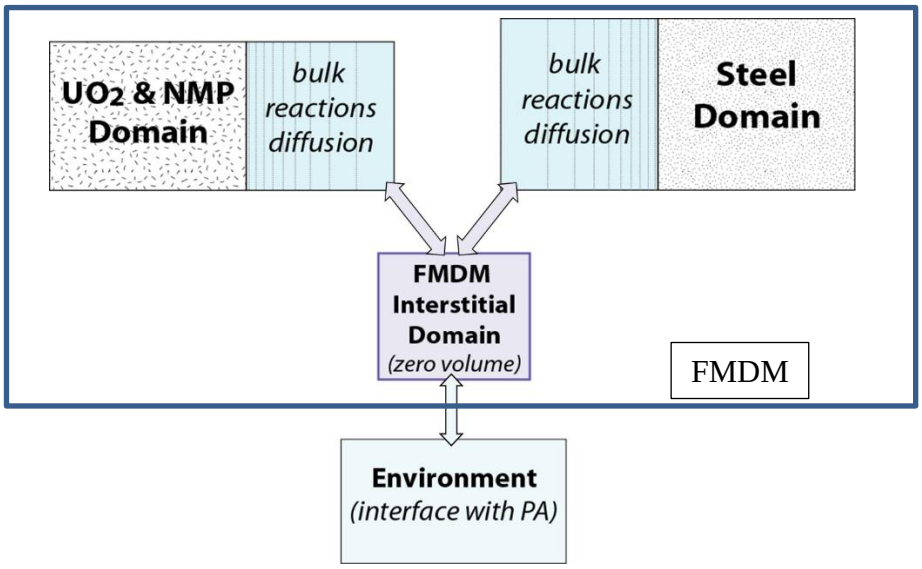

Figure 7. Schematic diagram showing the logic for how the steel surface was added to the FMDM.

There are several advantages to the approach of incorporating a separate steel corrosion module directly into the FMDM as shown in Figure 7:

- It directly couples fuel degradation and steel corrosion. This is vital, as it has been shown that, even at sub millimolar concentrations, the H_2 produced from the anoxic corrosion of steel can decrease the fuel dissolution rate by over four orders of magnitude (Jerden et al., 2015).
- directly coupling the fuel and steel degradation allows for the quantification of redox fronts that develop within the waste container due to the diffusion of radiolytic oxidants away from the fuel surface and the reactions of these oxidants with the steel surface and the resulting aqueous Fe^{2+} and H_2. This is also important because these redox fronts represent the Eh of the in-package solutions contacting the waste form and waste container internal components.
- This approach will allow the steel corrosion module to be readily implemented into the GDSA PA PFLOTRAN model, as it will be incorporated into the FMDM, a version of which has already been integrated with PA.

As shown in Figure 7 the steel environment (steel surface plus bulk solution) are coupled to the fuel environment through a zero-volume interstitial domain, which can exchange mass fluxes with

the fuel environment, the steel environment and the groundwater chemistry within the engineered barrier system adjacent to the waste package.

Within the FMDM no chemistry occurs in the interstitial domain or environment; those regions are zero-volume and only serve to provide an interface/outlet for the active fuel/NMP and steel domains. It is possible to control the interaction between domains by altering (1) the environmental concentrations, (2) the relative total areas of the two reactive domains, and/or (3) the leak rate from the interstitial domain to the environment. The environment domain serves as the input/output interface with the GDSA performance assessment model (the FMDM - PA interface is discussed in more detail below).

In parallel with the addition of the steel surface to the FMDM, the model parameter database was reviewed and updated. As part of this updating process several data gaps were identified to provide priorities for FY-2017 and future work. The main FMDM parameters and the important data gaps are summarized in Table 1.

Table 1. Summary of FMDM parameters and data gaps that need to be addressed in future work to improve the accuracy of the model.

Parameter	Description	Data needs to improve accuracy
Dimension of fuel environment	(mm – cm)	To be updated when dimensions of waste package are known
Nodes in fuel environment	(log-space grid: fine-spacing near surface)	To be updated when dimensions of waste package are known
Fuel surface coverage by NMP	(~1%)	From literature
Dimension of steel environment	(mm – cm)	To be updated when dimensions of waste package are known
Nodes in steel environment	(log-space grid: fine-spacing near surface)	To be updated when dimensions of waste package are known
Number of FMDM time steps	(100 – 1000)	Use to optimize PA interface
Fuel alteration layer porosity	(~50%)	From literature
Fuel alteration layer tortuosity	(~0.01)	From literature
Fuel alteration layer radiolysis factor	(*not used*)	*Could be activated to account for radionuclide uptake by U secondary phases*
Alpha particle penetration depth	(35μm)	From literature
Fuel burnup	(25 – 75 GWd/MTU)	Input from PA
Age of fuel (time out of reactor)	30 – 100 yrs	Input from PA
Resistance between fuel and NMP domains	(10^{-3} Volts/Amp)	Interpretation of literature
Temperature history	function	Data need: needs to be input from PA – will depend on repository scenario
Dose rate history	function	Based on MCNPX results of Radulescu, 2011
Spatial dose rate	function (decrease in dose rate with distance from fuel)	Based on MCNPX results of Radulescu, 2011
Rate constants for interfacial reactions in fuel and steel domains	See Figure 6 for summary of specific reactions	Data need: experiments needed due to lacking or inconsistent data in current literature on H_2 reactions on fuel and NMP and steel corrosion under relevant conditions
Charge transfer coefficients for interfacial half-cell reactions in fuel and steel domains	See Figure 6 for summary of specific reactions	Data need: experiments needed due to lacking or inconsistent data in current literature on H_2 reactions on fuel and NMP
Activation energys	T dependence: See Figure 6 for summary of specific reactions	Data need: experiments needed due to lacking or inconsistent data in current literature on H_2 reactions on fuel and NMP and steel corrosion under relevant conditions

Table 1. Continued.

Parameter	Description	Data needs to improve accuracy
Standard potentials for interfacial half-cell reactions: fuel and steel	See Fig. 6 for reactions	From literature
Relative area of fuel domain	Default 1:1, depends on waste package design	To be updated when dimensions of waste package are known
Relative area of steel domain	Default 1:1, depends on waste package design	To be updated when dimensions of waste package are known
Environmental leak rate (diffusion barrier factor)	Depends on waste package design, breach	Interpretation of literature
Environmental concentrations	(O_2, H_2, CO_3^{2-}, Fe^{2+})	Input from PA
Rate constants for bulk solution reactions in fuel, steel environments	See Figure 6 for summary of specific reactions	From literature
Activation energy for bulk solution reactions	T dependence, See Figure 6 for reactions	From literature
Passivation potential of steel surface	(85 V_{SCE}) as place-holder	Data need: experiments needed due to lacking or inconsistent data in current literature
Passivation corrosion current density	Calculated internally within FMDM	Function derived from literature
Radiolytic oxidant (H_2O_2) generation value (G_{cond})	Analytical function for conditional G_{H2O2} value from PNNL radiolysis model	Values based on radiolysis model results, Buck et al., 2013. *Would need to be updated, expanded for brine solutions (Cl, Br)*

3. RESULTS FROM TEST RUNS OF FMDM WITH STEEL CORROSION MODULE AS THE SOURCE OF HYDROGEN

A series of model runs were done using the updated FMDM over a range of relevant conditions assuming that the steel surface was pure iron metal (simulating carbon-steel). The focus of these runs was to quantify the sensitivity of the FMDM-predicted fuel degradation rate to the rate of steel corrosion. The conditions for these sensitivity calculations are listed below and examples of results are shown in Figures 8, 9 and 10.

- The variables that were changed for these sensitivity runs were: the interfacial rate constant for the oxidation of iron (reaction 1 below) and the age of the fuel.
  - The rate constant was varied from 10^{-3} to 1.0 mole/m^2yr (the actual value of this key parameter for different types of steels needs to be determined experimentally).
  - The age of fuel was varied from 20 to 200 years.
- Parameter values (see Table 1) for the fuel environment are from Jerden et al., 2015.
- Parameter values (see Table 1) for the steel environment are from King and Kolar, 2003.
- The environmental concentrations (constant concentration boundary) were $[H_2] = 10^{-15}$ M, $[O_2] = 10^{-9}$ M, $[Fe^{2+}] = 10^{-9}$ M, $[CO_3^{2-}] = 10^{-6}$ M.
- Temperature was held constant at 40^{o}C for all runs.

- Fuel burnup was 50 GWd/tHM (gigawatt days per metric ton of initial heavy metal: U).

At the corrosion potential of carbon steel, under anoxic conditions, the corrosion rate-determining half-reactions are:

$Fe^0 \rightarrow Fe^{2+} + 2e^-$ (1)
$2H_2O + 2e^- \rightarrow H_2 + 2OH^-$ (2)

Mixed potential theory states that, at the corrosion potential, the net sum of the current densities of all anodic and cathodic reactions equals zero. That is, the corrosion potential is defined as the kinetic balance between anodic and cathodic reactions. Therefore, since (1) and (2) are the dominant reactions on the corroding steel, the rate of H_2 generation will equal the rate of steel corrosion (Fe oxidation) in units of moles H_2 per steel surface area per time at the corrosion potential. So the steel corrosion rates shown in Figures 8, 9 and 10 are directly proportional to the H_2 generation rates.

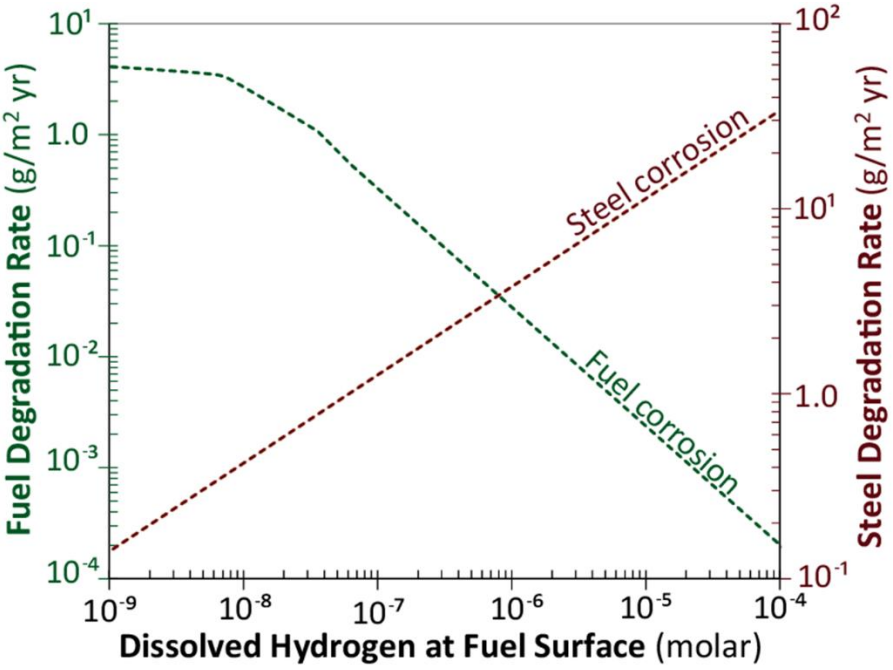

Figure 8. Used fuel and steel corrosion rates as functions of the concentration of dissolved H_2 in the common solution. This example is for a 200 year old fuel with a burnup of 50 GWd/tHM. The source of H_2 is the corrosion of steel and is thus its concentration is proportional to the steel corrosion rate (shown in red). For example, at a steel corrosion rate of ~$1.5x10^{-1}$ g/m^2 yr the resulting dissolved H_2 concentration at the fuel surface is 10^{-9} molar and for a steel corrosion rate of ~30 g/m^2 yr the H_2 concentration at the fuel surface is 10^{-4} molar.

Figure 8 indicates that, over a relevant range of steel corrosion rates, the concentration of dissolved H_2 that reaches the fuel surface can vary considerably. The variation in H_2 concentrations produced by this range of steel corrosion rates causes the predicted fuel degradation rate to vary

from $2x10^{-4}$ g/m^2 yr up to 4.0 g/m^2 yr over a range of nanomolar to 0.1 millimolar H_2 concentrations.

Figures 9 and 10 show the fuel degradation rates as a function of time when coupled with a range of relevant steel corrosion rates. The dashed curves in Figure 9 show the combined effects of radiolysis and steel corrosion and the solid curve shows the effects of radiolysis alone. As mentioned above, for this simple but relevant case of carbon steel corrosion, the rate of iron oxidation is equal to the rate of H_2 production at the steel surface. The fuel degradation rate decreases slowly with time as the dose rate at the fuel surface decreases due to the decreasing production rates of the radiolytic oxidant H_2O_2 and associated O_2. That is, as the amount of radiolytic H_2O_2 decreases it takes less H_2 to anodically protect the fuel from oxidative dissolution. Therefore, the fuel degradation rate decreases to the chemical dissolution rate near 10^{-4} for all steel corrosion rates (see Figure 6 for reaction schematic).

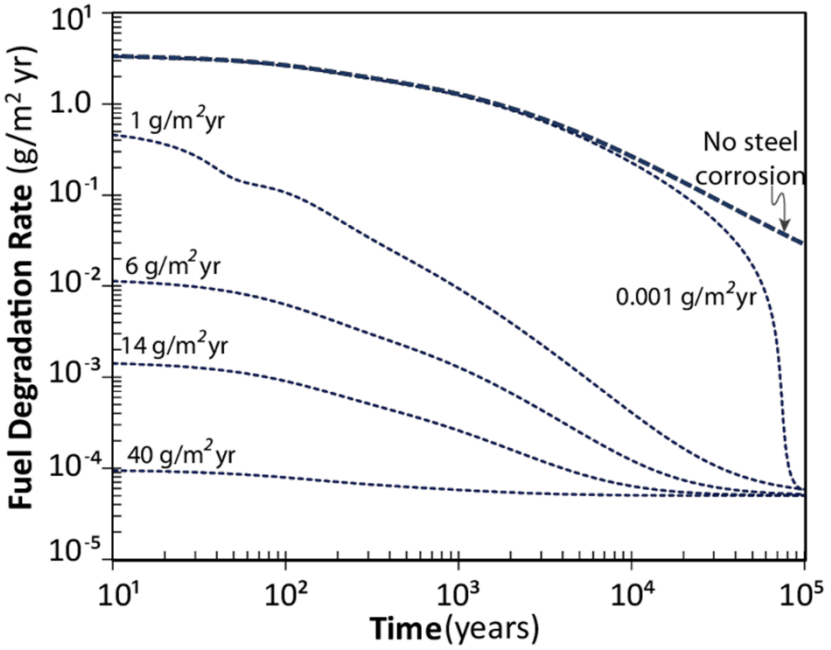

Figure 9. Results from the FMDM with the newly added steel corrosion module. All of these runs are for a 10 year old fuel with a burnup of 50 GWd/tHM. The rate of fuel degradation decreases with increasing steel corrosion rates due to the effect of H_2 which is produced at a rate proportional to steel corrosion (see Figure 6 for reaction summary).

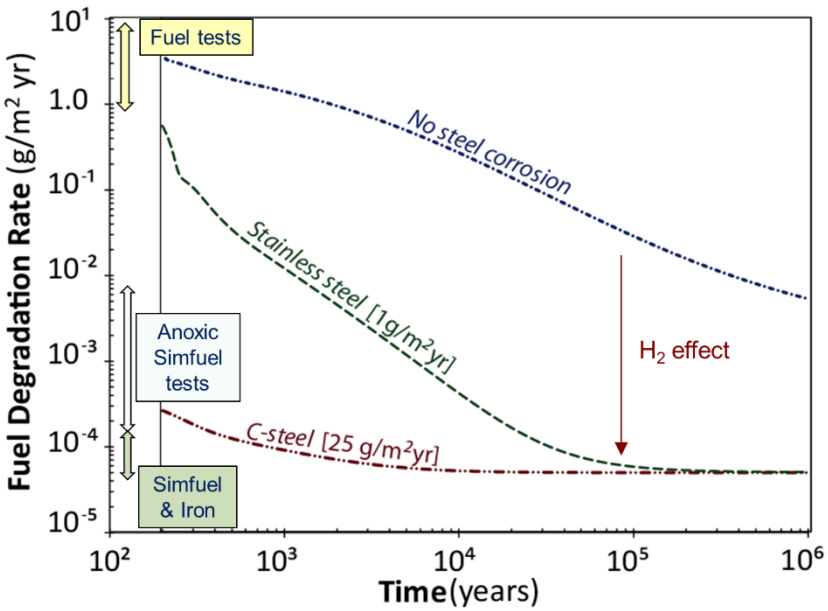

Figure 10. Results from the FMDM with the newly added steel corrosion module, comparing predictions with experimental ranges of degradation rates from relevant used fuel and simfuel tests. Fuel data from Cunnane 2004, Simfuel (U^{233} in UO_2) data from Ollila, 2008. These runs are for a 200 year old fuel with a burnup of 50 GWd/tHM.

Figure 10 also shows data ranges for used fuel and simulated fuel immersion tests. The fuel tests, compiled by Cunnane, 2004, were performed in oxidizing conditions using ~30 year old fuel that varied in burnup from 25 to 45 GWd/tHM. The temperature for these tests was varied from 25°C to 80°C, the pH varied from 7 to 9 and the solution was a buffered DIW with varying concentrations of dissolved carbonate (zero to millimolar). The simfuel tests (Ollila, 2008) involved the immersion of ^{233}U doped UO_2 in buffered DIW at pH 7 – 9 and 25°C to 90°C. These tests were performed under both anoxic conditions (argon purged) and reducing conditions (metallic iron added to tests).

The main conclusion drawn from Figure 10 is that, while there remains a need for focused electrochemical experiments to both measure parameter values and provide model validation data sets for the FMDM, it is encouraging that our initial results are roughly consistent with the data sets summarized in Figure 10 (within the test durations, which is on the order of months).

In order to assess the impact that the steel corrosion/H_2 effect will have on radionuclide source term calculations a hypothetical example was implemented using the radionuclide inventory for a 50 GWd/tHM BWR fuel provided by Carter et al., 2012. For this calculation the fuel dissolution rates from Figure 10 were multiplied by an assumed fuel specific surface area (9.5×10^{-4} m^2/g for fuel pellets in a typical BWR assembly, from Fillmore, 2003) to provide the fractional dissolution rate and then by the radionuclide inventory. For the example plots shown in Figures 11 and 12, the calculated activities of all isotopes were multiplied by biological toxicity factors from 10 CFR, Part 20, Appendix B.

Figure 11a shows the radionuclide source term for a case where there is no steel corrosion occurring during used fuel degradation (top line in Figure 10). Figure 11b shows a case that

assumes that the first 30,000 years of fuel degradation is accompanied by carbon steel corrosion that generates relatively high H_2 concentrations (~10^{-4} molar) within the waste package. The discontinuity at 30,000 years indicates the time at which all of the carbon steel has been consumed leading to the cessation of H_2 production and a corresponding increase in fuel dissolution rate. The time at which the carbon steel was all consumed was arbitrarily chosen and is likely unrealistic; however, it is still instructive in a qualitative sense to show how the consumption of steel can influence source term due to the H_2 effect.

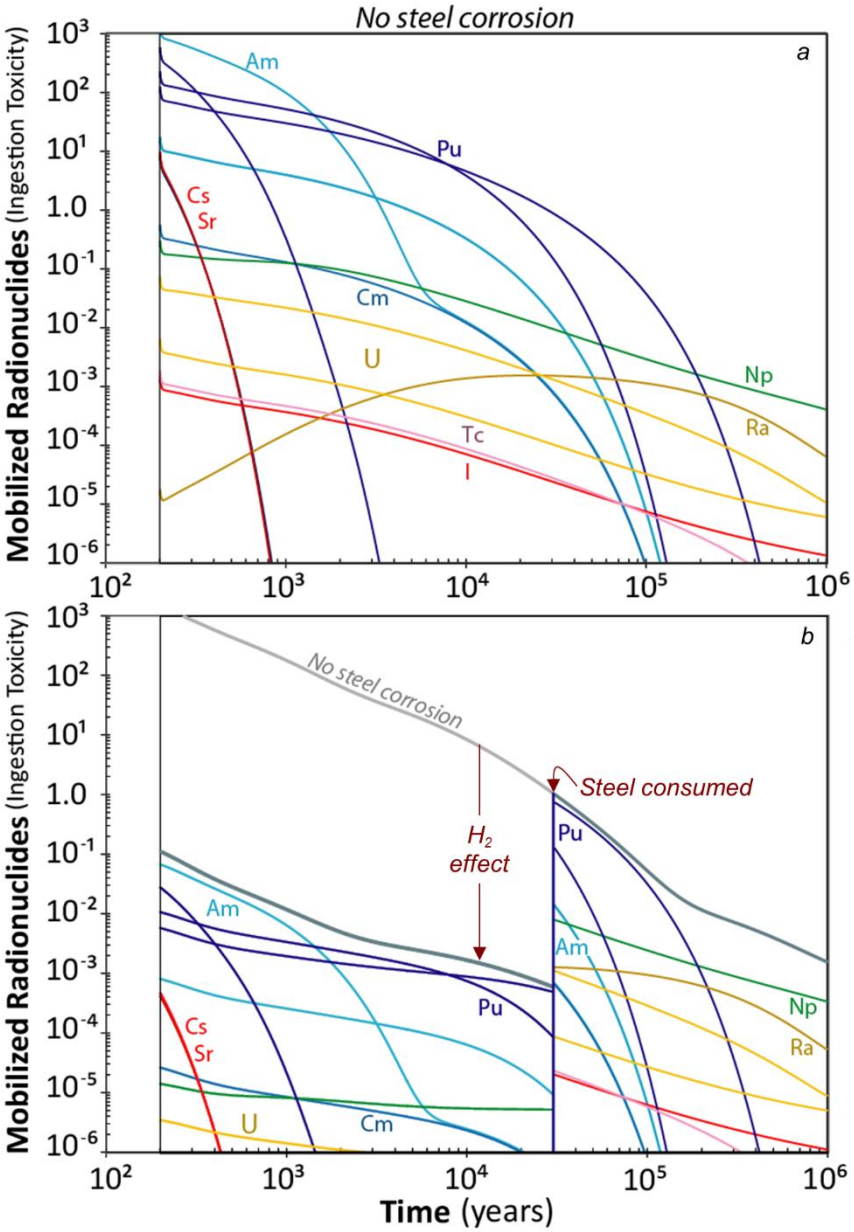

Figure 11. Hypothetical radionuclide source term for (a) the case with no steel corrosion, that is no H_2 generation during fuel degradation and (b) a case where carbon steel is corroding simultaneously with the used fuel for the first 30,000 years of the run. This example is for a 200 year old fuel with a burnup of 50 GWd/tHM. Specific isotopes are not labeled because the purpose of the plot is highlight the elemental output of this hypothetical source term example.

Perhaps a more realistic case is shown in Figure 12. In this figure it is assumed that carbon steel corrodes at a rate of 25 g/m^2 yr until it is all consumed at 3,000 years. At this point the more slowly corroding stainless steel (1 g/m^2 yr) dominates H_2 production rates resulting in a higher fuel degradation rate relative to the first 3,000 years. All steel assumed to be consumed by 40,000 years, resulting in the increase of fuel degradation rates due to the absence of H_2. Nevertheless, the benefit of accounting for steel corrosion in the FMDM calculations is revealed by integrating the curves to calculate the total mass that has dissolved.

Although the time frames for the FMDM test runs shown in Figures 11 and 12 are arbitrary and both the steel and fuel reaction parameters need to be validated by experiments, these hypothetical source term examples are qualitatively instructive. The most important observation is that, due to the H_2 effect, the radionuclide source term may be significantly attenuated. This indicates that having an accurate model for steel corrosion and the associated H_2 effect is essential for accurate source term calculations within the performance assessment model.

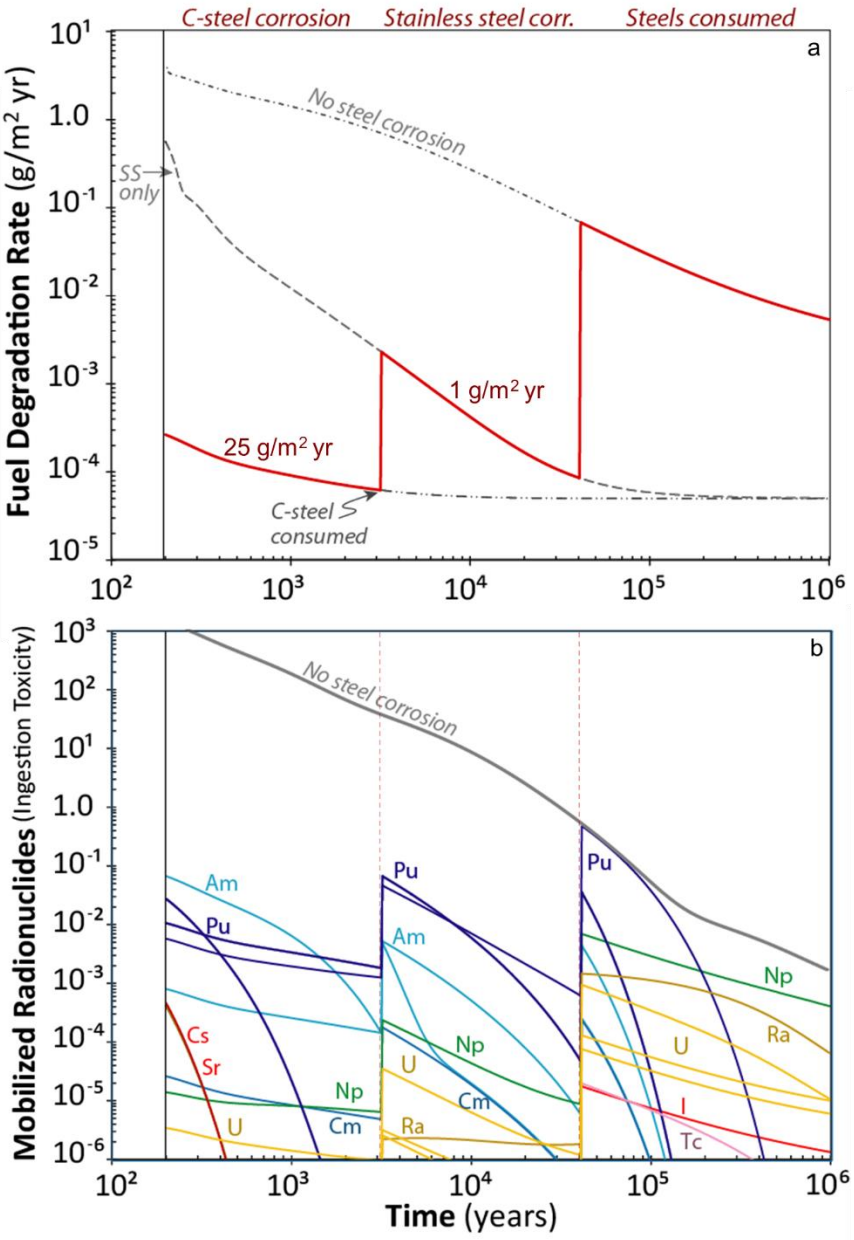

Figure 12. Hypothetical radionuclide source terms for the case where carbon steel corrosion dominates the first 3,000 years, followed by stainless steel until 40,000 years at which point all steel has been consumed (a). 12b shows the radionuclide source term for the case diagrammed in 12a. This example is for a 200 year old fuel with a burnup of 50 GWd/tHM. Specific isotopes are not labeled because the purpose of the plot is highlight the elemental output of this hypothetical source term example.

4. INTEGRATION OF FMDM WITH THE GENERIC DISPOSAL SYSTEM ANALYSIS PERFORMANCE ASSESMENT MODEL

Although the basic calculations in the FMDM were successfully integrated with GDSA PA reactive transport code PFLOTRAN in FY-2015 (Jerden et al., 2015), there remains a need to extend the code to encompass all chemical processes relevant to source term (e.g., the addition of the steel corrosion as a source of H_2) and optimize the FMDM code to improve performance. In addition to the extension of the FMDM to include the steel corrosion module (see Section 2 above), the FY-2016 integration work also focused on optimizing the FMDM code.

The basic information flow involved in the integration of the FMDM with PFLOTRAN is shown in Figure 13.

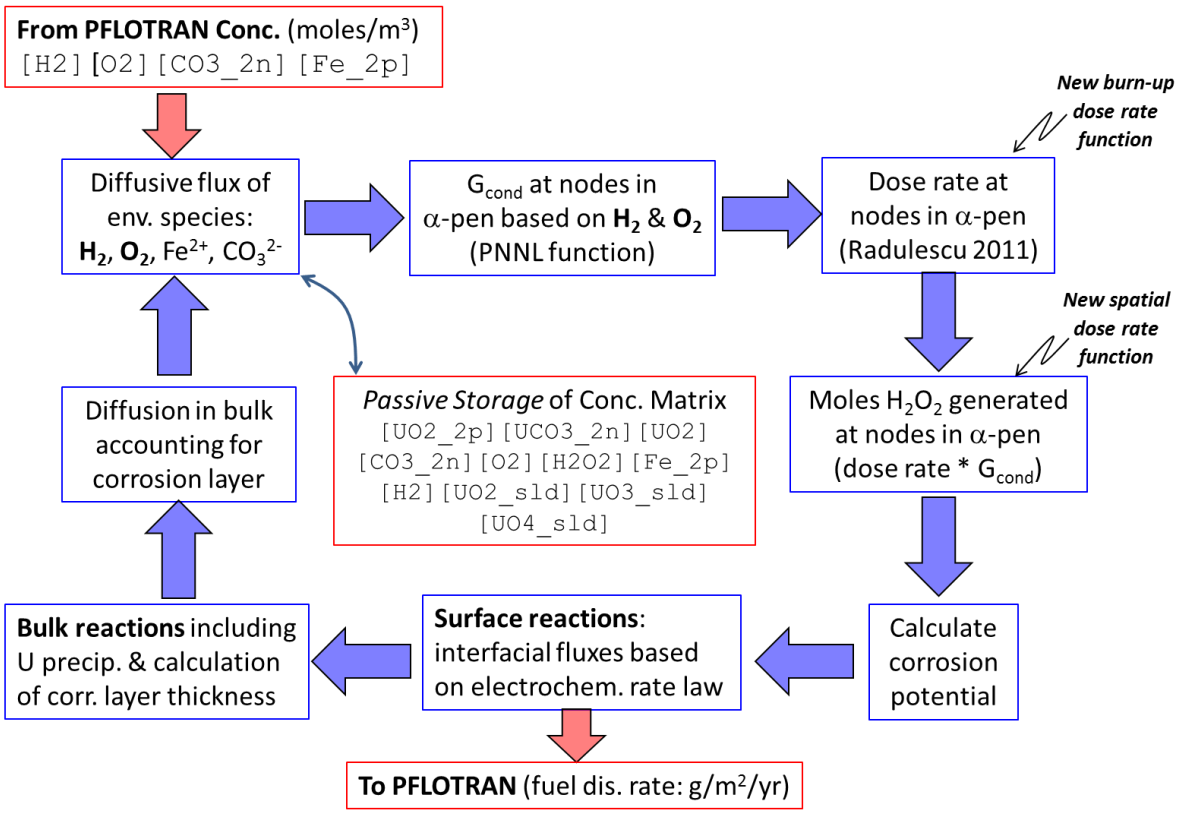

Figure 13. Conceptual flow diagram showing the individual calculations within a single time step of the FMDM. Note that the concentrations of all components must be stored and fed back to the FMDM at the beginning of each new time step. G_{cond} refers to the conditional generation value for H_2O_2, which determines the peroxide generation rate within the alpha radiation zone (α–pen). In the FMDM v.2.3 the conditional H_2O_2 generation value is calculated by an analytical function (G_{cond} is a function of $[H_2]$ and $[O_2]$).

The FY-2016 FMDM (V.3) optimization work involved the following activities:

- The dose rate function was re-conditioned to avoid mathematical instability.
- Because Code profiling and sensitivity runs showed that the majority of the computing time of the FMDM is taking place in the bulk chemical reaction module, a plan for streamlining the reaction diffusion equations used in this module was formulated.
- A conceptual plan for integrating the FMDM (V.3) into PFLOTRAN was developed and is summarized in Figures 14 and 15 below.

Update of burnup (BU) - dose rate (RAD) function: The dose rates extrapolated to the fuel surface (distance equals zero) were correlated with the results of Radulescu 2011. The dose rate correlation from the Jerden et. al., 2015 report was replaced because of concerns with non-smooth transitions. For the new dose rate function, the main dose profile is represented using a logistic function, and the Am-241 in-growth was accounted for using a Gaussian. This expression should be globally valid, as long as the burn-up and age-of-fuel are greater than zero.

Figure 14 shows how the six process modules that make up the FMDM (V.3) are related to the GDSA PA model. All of the modules are coupled and the flow of information between them is summarized in Figure 13. The primary output of the FMDM is the fuel degradation rate in mass per surface area per time, which is used to define the radionuclide source term in PFLOTRAN. in addition to numerical inputs and outputs between FMDM and PFLOTRAN shown in Figure 14, there are also a number of places where model parameters need to be coordinated to avoid internal inconsistencies within the PA calculation. These points of coordination include:

- Time at which the waste package is breached.
- The temperature history of the waste package.
- The radionuclide inventory used in PFLOTRAN needs to be consistent with the burnup used in the FMDM.
- The solubility limits used in PFLOTRAN need to be consistent with the solubility limits for U(VI) secondary phases and iron oxides used in the FMDM.
- The specific surface area assumed in the PFLOTRAN source term model needs to be consistent with the relative surfaces of the fuel, steel and NMP domains within the FMDM.

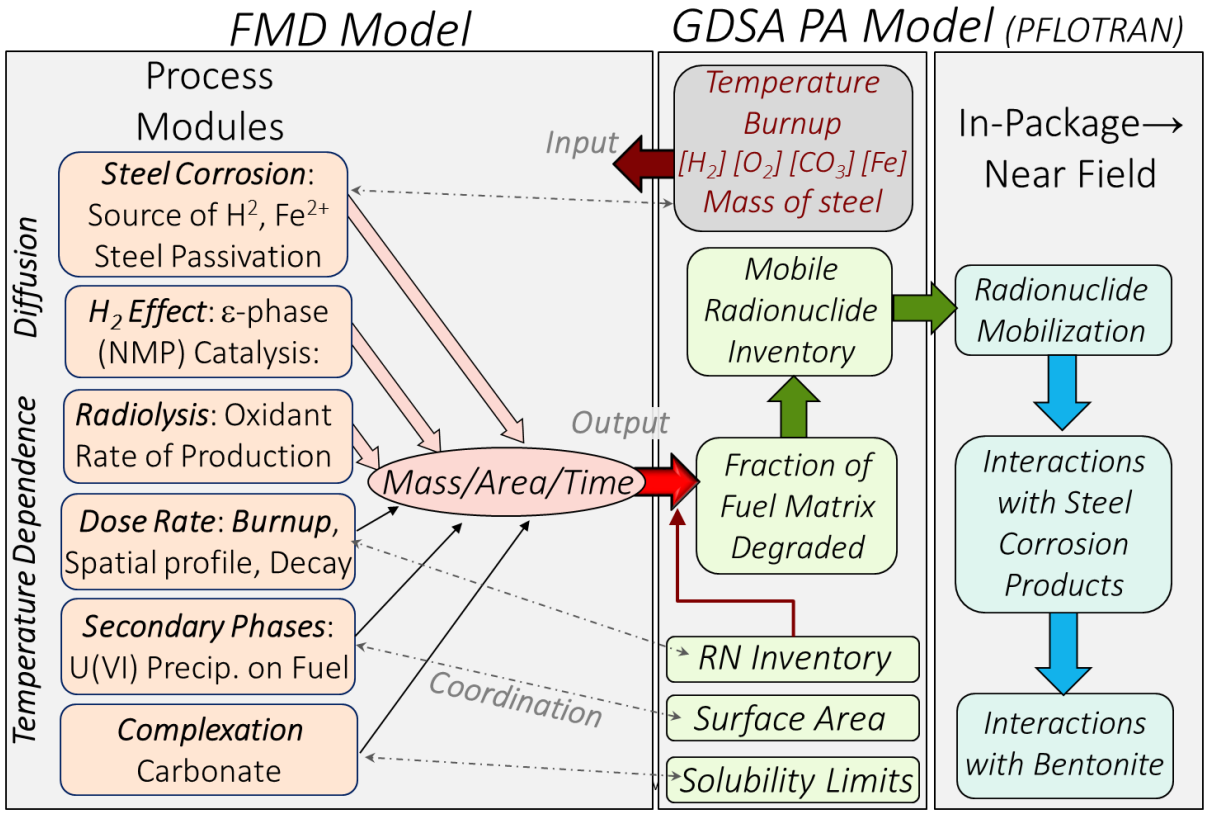

Figure 14. Conceptual diagram showing all of the active process modules in the latest version of the FMDM (V.3) and how they are integrated in terms of inputs and outputs with the PA model.

Figure 15 highlights the key objectives of work proposed for FY-2017 in the context of model integration. As discussed in this report, the effect of H_2 produced from the anoxic corrosion of steel will likely dominate the radionuclide source term for relevant repository scenarios. FY-2017 work will focus on quantifying parameter values and calibrating the steel corrosion and H_2 effect modules that are currently in the FMDM. This work will be done in parallel with efforts to optimize the serial performance of the FMDM to minimize run times. Once these modules are appropriately parameterized and tested, they will be added to the FMDM Fortran files that are called by PFLOTRAN to run within the GDSA PA model.

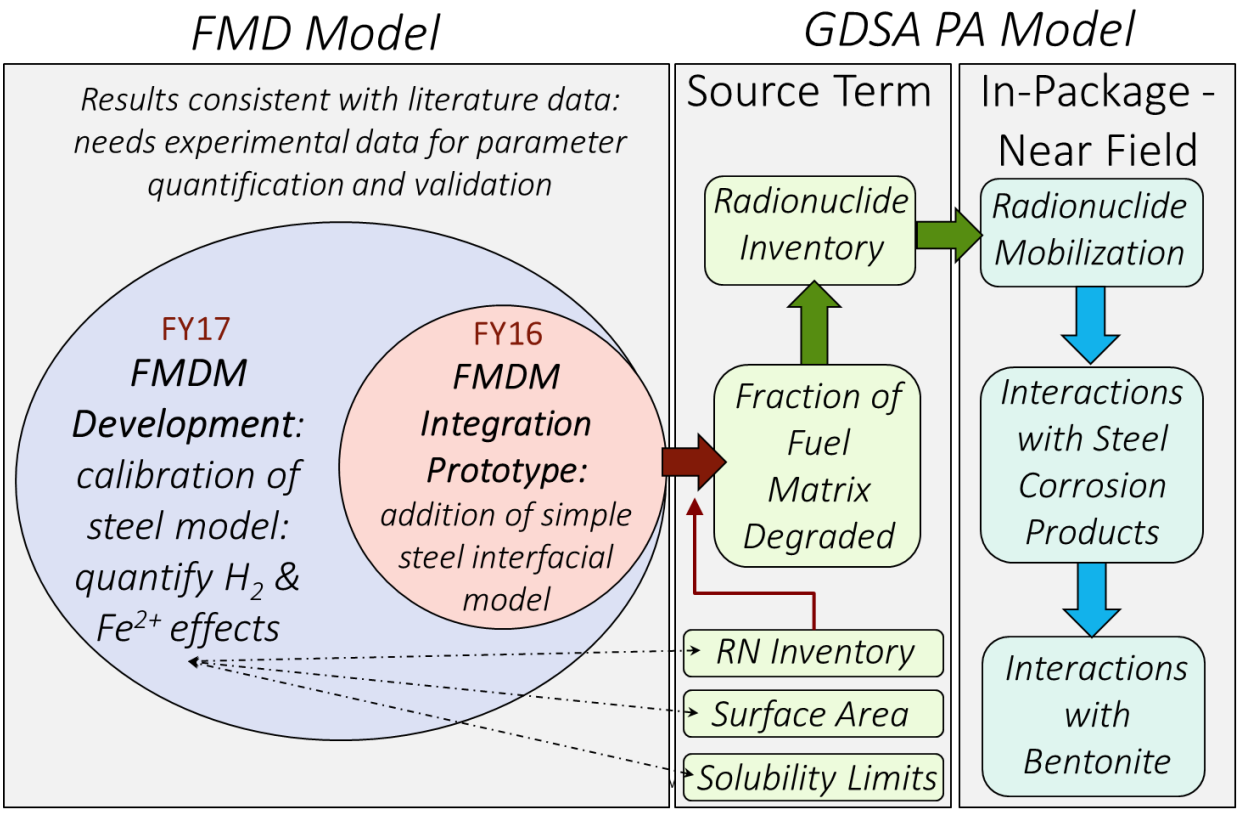

Figure 15. Conceptual diagram highlighting the major objective for FY-2017 in the context of integration with the GDSA PA modeling work.

5. RESULTS FROM SCOPING EXPERIMENTS ON POISONING CATALYTIC ACTIVITY OF NOBLE METAL PARTICLES

To ensure that the process modules for used fuel degradation and steel corrosion accurately represent reality within the relevant ranges of repository conditions, the model development efforts need to be coupled with a focused experimental program to quantify key parameters and provide data sets for validation. Although the FY-2016 scope for this project did not include a deliverable for experimental work, scoping tests were performed using the radiological electrochemical testing facilities at Argonne to provide confidence that the effect of H_2 on used fuel degradation is accurately represented in the FMDM and thus in the PA model.

As shown in Jerden et al., 2015, and in Section 2 above, the catalysis of H_2 oxidation on the NMPs attenuates the used fuel dissolution rate by as much as four orders of magnitude when dissolved H_2 concentrations reach approximately 0.1 mM. Because this NMP – H_2 catalysis process plays such a key role in determining the fuel dissolution rates and its mechanism is not yet fully understood, it is the subject of on-going electrochemical experiments designed to directly inform the process modeling efforts.

The experimental set up for the scoping tests consists of a 20 mL, three-electrode cell in which the experimental cover gas is continuously bubbled during the experiments (Figure 16). Multiple cells (experiments) are run simultaneously within an oven in a radiological laboratory. Multiple power supplies and potentiostats are available so that tests with two or more working electrodes (e.g., NMP and UO_2) can also be performed. The electrodes are characterized pre- and post-experiment by optical and Scanning Electron Microscopy (SEM). The solutions from selected tests are analyzed for electrode constituents (Ru, Mo, Pd, Rh, Tc, U, and other dopants such as REE) by Inductively coupled plasma mass spectrometry (ICP-MS).

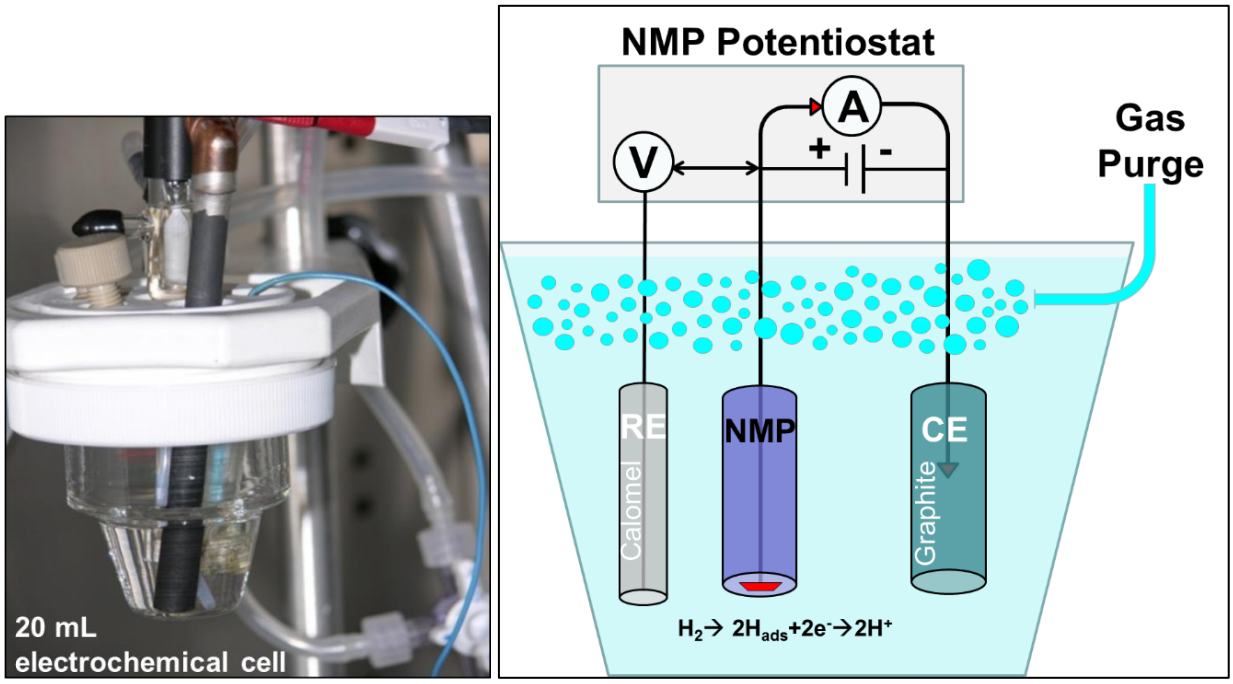

Figure 16. Photograph and schematic diagram of the type of cell used for the electrochemical experiments.

Tests performed in FY-2015 through FY-2016 focused on the interfacial reactions of H_2 with electrodes composed of a technetium bearing noble metal partial, which serves as a simulant for the fission product alloy present in spent fuel and modeled in the FMDM (NMP on Figures 2 and 6 above). Other tests were performed with electrodes made of the most abundant pure elements present in the NMP (Ru, Mo, and Pd). The NMP simulant electrode was made in house (Argonne) from an alloy produced by Steve Frank at Idaho National Laboratory that closely matches the composition and homogeneity (single alloy phase) of the NMP (ε-phase) found in used fuel. The NMP alloy used to make the electrode has a composition of $Ru_{56}Mo_{20}Rh_{11}Pd_{11}Tc_2$ and, based on characterization by SEM and energy dispersive x-ray analyses (EDS), appears to be composed of a single phase with trace amounts of TcO_2.

The EDS analyses of several locations on the NMP alloy used in our experiments show that this material falls within the compositional range of the fission product alloys generated in UO_2 light water reactor fuels (Figure 17).

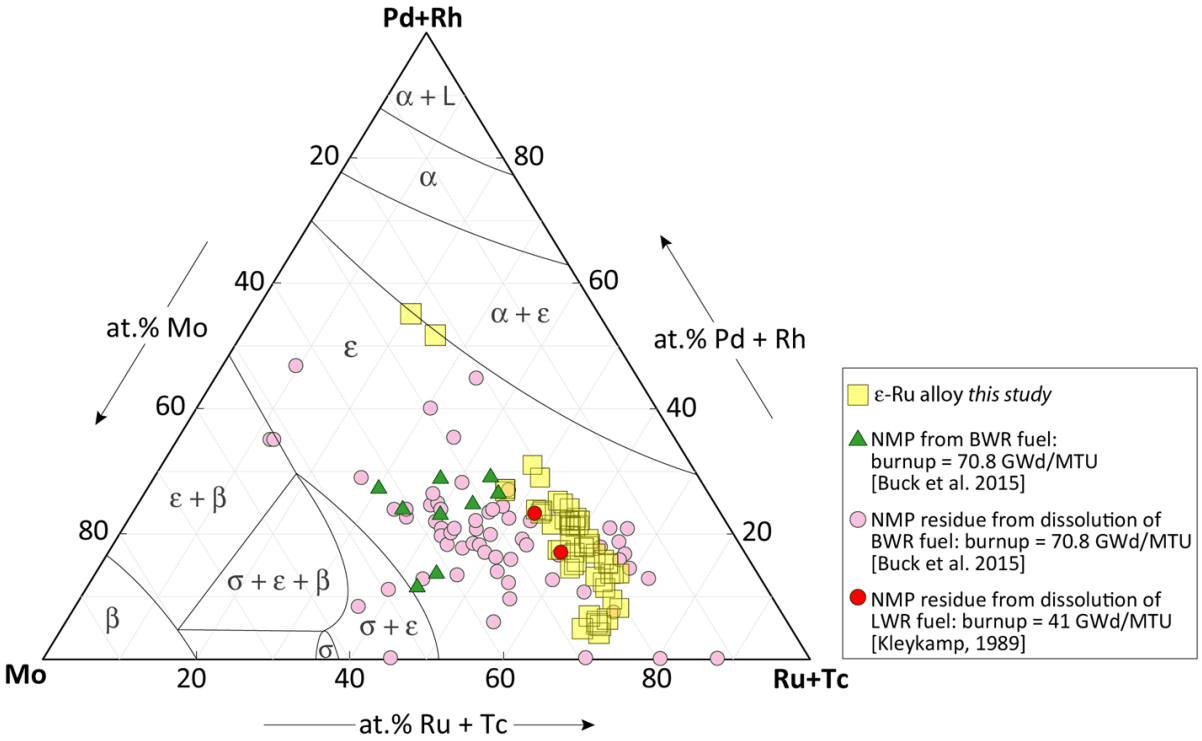

Figure 17. Energy dispersive x-ray analyses of the NMP alloy used in the scoping experimental studies (yellow squares). Note that the alloy falls within the ε-Ru phase field and is thus representative of the fission product alloy phase present in used fuel. The phase fields are for the 1700°C plot of this system from Kleykamp, 1989.

One of the most important experimental observations made regarding the role of H_2 in used fuel dissolution is that the presence of dissolved halides, particularly Br^-, seems to counteract the H_2 effect (Metz et al., 2008). Although the mechanism is poorly understood, our new results (Figure 18) suggest that the NMP surfaces may be poisoned by halides and reduce their catalytic efficiency (i.e., counteract the protective H_2 effect). The effects of poisoning and alteration of the NMP surfaces are not currently accounted for in the FMDM, because these processes are not well understood or quantified. However, due to the importance of the H_2 effect these processes are deemed high priorities for experimental investigations.

To investigate the reaction of H_2 on the NMP and other metal electrodes, scoping tests were performed in which the open circuit potential (OCP) of the electrode was measured for up to 80 hours in 1 mM NaCl purged by bubbling either air, Ar or 2% H_2 in Ar through the solution. The possible poisoning effect of Br^- was also investigated by performing the 2% H_2 cover gas tests in solutions containing 1 mM NaBr. The pH for all tests remained relatively constant at around 7.0. Typical results are shown in Figure 18.

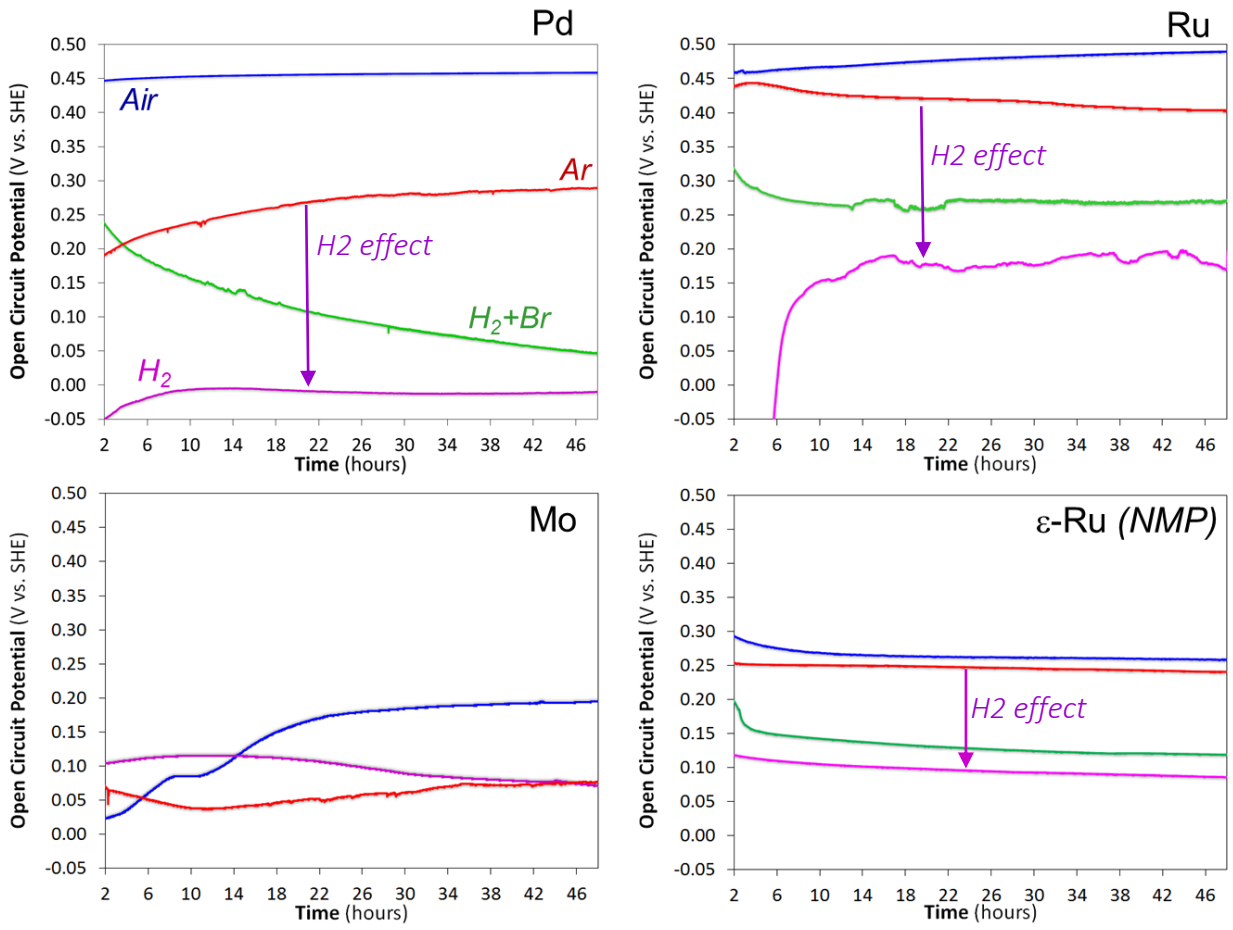

Figure 18. Results from scoping electrochemical tests showing the open circuit potentials of the $Ru_{56}Mo_{20}Rh_{11}Pd_{11}Tc_2$ (NMP) and pure Pd, Ru and Mo electrodes in 1 mM NaCl solution purged with air (blue curves), Ar (red curves), or H_2/Ar (violet curves) and 1 mM NaCl + 1 mM BrCl solution purged with H_2/Ar (green curves). Note that the presence of Br^- partially counteracts the H_2 effect on all of the electrode materials except for Mo. The Mo results were inconsistent due to the formation of an oxide layer (MoO_2) during the test.

The results of tests with the NMP electrode show a pronounced H_2 effect that causes a decrease in the open circuit potential from greater than 260 mV (vs. SHE) for the air cover gas tests down to around 100 mV for tests performed with 2% H_2 in Ar as the cover gas. That this large potential drop is not seen when the test is performed in pure Ar indicates that it is due to H_2 oxidation occurring on the NPM electrode. This shows that, under near neutral conditions, the NMP surface is hosting anodic reactions that can be generalized as:

$$H_2 \rightarrow 2H_{adsorbed} + 2e^- \rightarrow 2H^+ \quad (4)$$

As indicated by the green curves in Figure 18, the presence of 1 mM Br^- partially counteracts the H_2 effect, resulting in the NMP surface potential being approximately 60 mV higher than in its absence. The relative effects of both H_2 and Br^- on the OCP are significantly greater for reactions on the Ru and Pd electrodes; however, the results for the Mo electrode are confounded by the

growth of an oxide layer (MoO_2) during the tests. It is likely that a thin (undetectable by SEM) MoO_2 layer is generated on the NMP electrode during the test.

Figure 19 shows the Eh – pH diagrams for the main constituents of the NMP. Of particular interest in Figure 19 is the observation that the MoO_2 stability field overlaps the field for repository relevant conditions. This if interest because it implies that Mo within the NMP will likely oxidize when exposed to in-package solutions, which may impact the catalytic activity of the NMP surfaces. The Eh – pH diagrams also indicate that sulfur may play an important role in the surface chemistry of Ru (the dominant element in the NMP) and thus should be accounted for in future experimental and modeling efforts.

Figure 19 also indicates that MoO_2 and perhaps Ru sulfides could play an important role in the evolution of the NMP surfaces under repository relevant solutions. This is important because the NMP surfaces are responsible for the H_2 effect that anodically protects used fuel from oxidation (see Figure 7 above). This indicates that future experimental and modeling efforts should account for the evolution of the NMP surface in relevant solutions.

The results in Figure 18 also show that even over short time frames (minutes) the presence of Br^- has an effect on the NMP – H_2 reaction. This is a significant observation as it identifies a key chemical process, that could counteract the protective H_2 effect that is not currently accounted for in the FMDM.

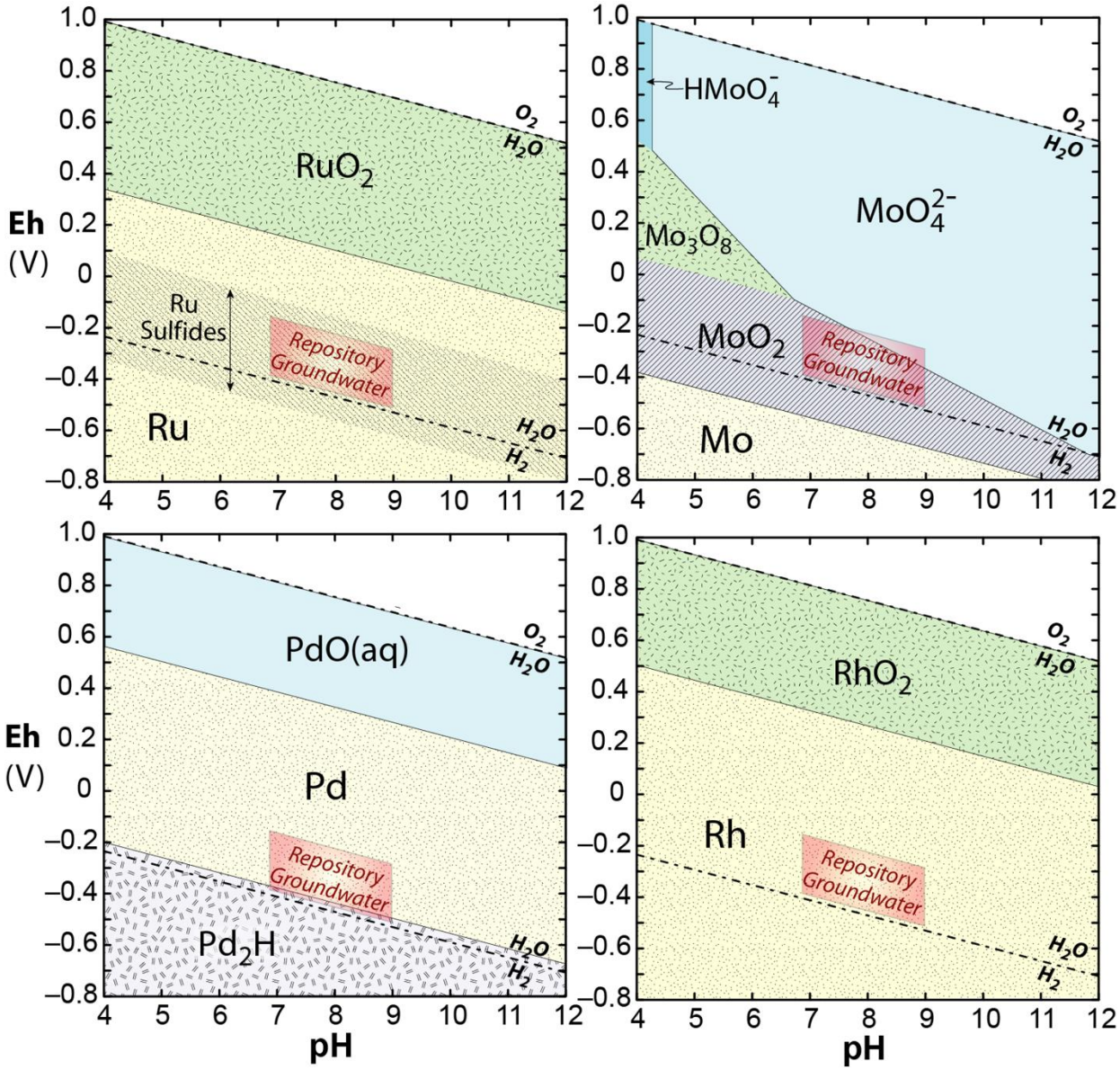

Figure 19. Eh – pH diagrams for the major constituents of the noble metal particle alloy (NMP) present in used fuel.

Future experimental work will also involve a series of electrochemical tests with simulated used fuel that consists of NMP in a UO_2 matrix. These tests will be used to generate a validation data set for the FMDM.

6. CONCLUSIONS AND RECOMMENDATIONS FOR FUTURE WORK

The primary purpose of this project is to develop a process model to calculate the degradation rate of used fuel based on fundamental underlying processes used to determine radionuclide source terms for reactive transport calculations in the Generic Disposal System Analysis PA model.

The main accomplishments for Argonne's FY2016 work on the Fuel Matrix Degradation Model (FMDM) development project are as follows:

- Formulated, coded and tested an electrochemical steel corrosion module that couples in-package steel corrosion with fuel degradation through the common solution. This module provides the kinetic source of H_2 that may control the used fuel dissolution rates under repository relevant conditions.
- Updated and optimized FMDM to improve the efficiency of integration with the GDSA PA model.
- Performed scoping electrochemical tests to build confidence in modeling the H_2 effect mechanism, which has been shown by both experiment and electrochemical modeling to significantly impact source term calculations when in-package steel components are corroding simultaneously with used fuel.

The key finding of the FY-2016 work was that the corrosion of steel canister materials will have a significant impact on the radionuclide source terms calculated by PA because of its role as the major source of the H_2, which attenuates the fuel degradation rate. The test runs with the updated FMDM indicate that the peak radionuclide source term from a breached waste package will likely be attenuated by the H_2 effect and the corrosion of steel components (the dominant source of H_2 in the system).

These processes have been added in the FMDM V.3; however, there remains a need for coupled experimental and process modeling work to accurately parameterize and validate the model. This future work is particularly important because the FMDM is currently being used to provide the radionuclide source term in the PA model. Thus, future improvements to the FMDM process model will have a direct impact on the accuracy of the existing GDSA PA model.

FY-2017 activities of particular importance are:

- Extend the FMDM Fortran – PFLOTRAN interface files to account for the corrosion of the steel components and the associated H_2 effect that anodically protects the fuel from oxidative degradation.

- Take next step in integration of FMDM with PA: demonstrate sensitivity of the Argillite PA model to key variables in the FMDM such as burnup, surface area, steel corrosion/H_2 production rates and the dissolved concentrations of H_2, O_2, carbonate and ferrous iron.
- Perform focused electrochemical experiments to determine the effect of halides and other possible poisons on the catalytic efficiency of the NMP. These tests will quantify processes that may counteract the protective H_2 effect.
- Account for the effect of poisons (e.g., Br, S) or other processes that counteract the protective H_2 effect in the FMDM.

Furthermore, the recognition and quantification of the interactions between the corrosion of steel waste package components and waste form degradation suggests that our models may provide important insights as to the types of steel that could be used to optimize the long-term performance of the waste package and canister materials.

7. REFERENCES

Buck E., Jerden, J., Ebert, W., Wittman, R., (2013) Coupling the Mixed Potential and Radiolysis Models for Used Fuel Degradation, FCRD-UFD-2013-000290.

Buck, E., Mausolf, E., McNamara, B., Soderquist, C., Schwantes, J., 2015, Nanostructure of Metallic Particles in Light Water Reactor Used Nuclear, *Journal of Nuclear Materials* 461, 2015, 236–243

Cunnane, J.C., 2004, CSNF Waste Form Degradation: Summary Abstraction, Bechtel SAIC Company LLC Technical Report, ANL-EBS-MD-000015 REV 02, August 2004

Fillmore, D.L., 2003, Parameter Selection for Department of Energy Spent Nuclear Fuel to be Used in the Yucca Mountain License Application, Idaho National Engineering and Environmental Laboratory Report, INEEL/EXT-03-01032 Revision 1, October 2003

Grambow, B., Bruno, J., Duro, L., Merino, J., Tamayo, A., Martin, C., Pepin, G., Schumacher, S., Smidt, O., Ferry, C., Jegou, C., Quiñones, J., Iglesias, E., Rodriguez Villagra, N., Nieto, J., Martínez-Esparza, A., Loida, A., Metz, V., Kienzler, B., Bracke, G., Pellegrini, D., Mathieu, Wasselin-Trupin, G., Serres, C., Wegen, D., Jonsson, M., Johnson, L., Lemmens, K., Liu, J., Spahiu, K., Ekeroth, E., Casas, I., de Pablo, J., Watson, C., Robinson, P., Hodgkinson, D., 2010, Model Uncertainty for the Mechanism of Dissolution of Spent Fuel in Nuclear Waste Repository, European Commission, Final Report for MICADO Project, EUR 24597, 2010.

Jerden J. Copple J., Frey K. Ebert W., 2014, Prototype Fortran Version of the Mixed Potential Process Model for Used Fuel Degradation, Used Fuel Disposition Campaign Milestone: M4FT-15AN0806012, October 15, 2014

Jerden J., Glenn Hammond, G., Copple J., Cruse, T., Ebert W., 2015, Fuel Matrix Degradation Model: Integration with Performance Assessment and Canister Corrosion Model Development, FCRD-UFD-2015- 000550, July 21, 2015

Jerden J. Frey K. Ebert W., 2015, A Multiphase Interfacial Model for the Dissolution of Spent Nuclear Fuel, *Journal of Nuclear Materials*, 462, 135–146

Joe T. Carter, J., Luptak, A., Gastelum, J., Stockman, C., Miller, A., 2012, Fuel Cycle Potential Waste Inventory for Disposition, FCR&D-USED-2010-000031 Rev 5, July 2012

King F. and Kolar M., (2003). The Mixed-Potential Model for UO_2 Dissolution MPM Versions V1.3 and V1.4., Ontario Hydro, Nuclear Waste Management Division Report No. 06819-REP-01200-10104 R00.

Kleykamp, H., Constitution and Thermodynamics of the Mo-Ru, Mo-Pd, Ru-Pd and Mo-Ru-Pd Systems, *Journal of Nuclear Materials*, 167 (1989), 49-63

Laaksoharju M., Smellie, J., Tullborg, E-L., Gimeno, M., Hallbek, L., Molinero, J., Waber, N., 2008, Bedrock hydrogeochemistry Forsmark site descriptive modeling SDM-Site Forsmark, SKB R-Report (R-08-47), SKB, Stockholm, Sweden

Mariner, P., Gardner, P., Hammond, G, Sevougian, D, Stein E., 2015, Application of Generic Disposal System Models, FCRD-UFD-2015-000126, SAND2015-10037, September 22, 2015, 209pp.

Metz V., Loida A., Bohnert E., Schild D., Dardenne K., (2008) Effects of Hydrogen and Bromide on the Corrosion of Spent Nuclear Fuel and γ-irradiated UO_2(s) in NaCl Brine, *Radiochim. Acta* 96, 637–648

NRC Regulations, Title 10, Code of Federal Regulations, PART 20—STANDARDS FOR PROTECTION AGAINST RADIATION, Appendix B to Part 20—Annual Limits on Intake (ALIs) and Derived Air Concentrations (DACs) of Radionuclides for Occupational Exposure; Effluent Concentrations; Concentrations for Release to Sewerage

Ollia, K., 2008, Dissolution of Unirradiated UO_2 and UO_2 Doped with ^{233}U in Low- and High-Ionic-Strength NaCl Under Anoxic and Reducing Conditions, Posiva Working Report 2008-50

Radulescu, G., (2011) Repository Science/Criticality Analysis, Oak Ridge National Laboratory, Reactor and Nuclear Systems Division, FTOR11UF0334, ORNL/LTR-2011, Oak Ridge National Laboratory, Oak Ridge, TN.

Röllin S., Spahiu K., Eklunda U., (2001), Determination of Dissolution Rates of Spent Fuel in Carbonate Solutions Under Different Redox Conditions with a Flow-through Experiment, *Journal of Nuclear Materials*, 297, 231–243

Shoesmith, D., 2008, The Role of Dissolved Hydrogen on the Corrosion/Dissolution of Spent Nuclear Fuel, Nuclear Waste Management Organization, Toronto, Ontario, Canada, TR-2008-19, November 2008.

Wang Y. et al., (2014) *Used Fuel Disposal in Crystalline Rocks: Status and FY14 Progress*, FCRD-UFD-2014-000060, SAND2014, Sandia National Laboratories, Albuquerque, NM.